BJR

Received: 1 February 2016 | Revised: 17 March 2016 | Accepted: 30 March 2016

http://dx.doi.org/10.1259/bjr.20160108

Cite this article as:
Jafar MM, Reeves J, Ruthven MA, Dean CJ, MacDougall ND, Tucker AT, et al. Assessment of a carbon fibre MRI flatbed insert for radiotherapy treatment planning. *Br J Radiol* 2016; **89**: 20160108.

FULL PAPER

Assessment of a carbon fibre MRI flatbed insert for radiotherapy treatment planning

[1,2]MAYSAM M JAFAR, DPhil, [1]JONATHAN REEVES, PhD, [1]MATTHIEU A RUTHVEN, MEng, [1]CHRISTOPHER J DEAN, MSc, MPhys, [1]NIALL D MACDOUGALL, PhD, [1,3]ARTHUR T TUCKER, PhD and [1,3]MARC E MIQUEL, PhD

[1]Clinical Physics, Barts Health NHS Trust, London, UK
[2]Barts Cancer Institute, Queen Mary University of London, London, UK
[3]William Harvey Research Institute, Queen Mary University of London, London, UK

Address correspondence to: Dr Maysam Mahmood Jafar
E-mail: *maysam.jafar@gmail.com*

All authors equally contributed to this paper with conception and design of the study, literature review and analysis, drafting and critical revision and editing, and final approval of the final version.

Objective: The purpose of this work was to assess heating and radiofrequency (RF) deposition and image quality effects of a prototype three-section carbon fibre flatbed insert for use in MRI.
Methods: RF deposition was assessed using two different thermometry techniques, infrared thermometry and Bragg-grating thermometry. Image quality effects were assessed with and without the flatbed insert in place by using mineral oil phantoms and a human subject.
Results: Neither technique detected heating of the insert in typical MRI examinations. We found that the insert was less suitable for MRI applications owing to severe RF shielding artefact. For spin-echo (SE), turbo spin-echo (TSE) and gradient-echo sequences, the reduction in signal-to-noise ratio (SNR) was as much as 89% when the insert was in place compared with the standard couch, making it less suitable as a patient-support material. Turning on the MultiTransmit switch together with using the scanner's quadrature body coil improved the reduction in SNR from 89% to 39% for the SE sequence and from 82% to 12% for the TSE sequence.
Conclusion: No evidence was found to support reports in the literature that carbon fibre is an unsuitable material for use in MRI because of heating.
Advances in knowledge: This study suggests that carbon fibre is less suitable for large-scale MRI applications owing to it causing severe RF shading. Further research is needed to establish the suitability of the flatbed for treatment planning using alternative sequences or whether an alternative carbon fibre composite for large-scale MRI applications or a design that can minimize shielding can be found.

INTRODUCTION

Radiotherapy centres are increasingly combining CT and MR images to better define soft-tissue cancer treatment targets. Patients need to be in near identical positions during imaging and treatment in both CT and MRI. Radiotherapy treatment couches are always flat to optimize patient reproducibility and include indexable positions to attach immobilization devices. Carbon fibre is an ideal material for such couches owing to its lightweight, strength and rigidity.[1] Jockisch et al[2] found carbon fibre-reinforced polyether ether ketone to be safe in rabbits and beagles while producing a non-specific foreign-body tissue reaction. Clinical MRI-compatible devices have also been made with carbon fibres.[3–8] Liney et al[3] compared induced image artefacts of 2-mm-diameter carbon fibre rods with MR-compatible needles for pre-surgical breast lesion detection in phantoms. Artefact-free visualization of the tip, which was within 1 mm of the desired target, was achieved with the carbon fibre rods. Ernstburger et al[4] assessed the susceptibility artefacts in MR images of three invertebral spacers each made of a different material (carbon, titanium and cobalt–chrome) at 1.5-T magnet field strength. A control spacer was made of the human cortical bone. They found that there were fewer susceptibility artefacts in the images of carbon spacers than in the images of other spacers. "The carbon, titanium and cobalt–chrome spacers scored 83.3%, 62.5% and 50%, respectively." Thomas et al[6] found that an MRI-compatible carbon fibre needle for MRI-guided musculoskeletal interventions created smaller susceptibility artefacts than a traditional titanium needle, which induces a large artefact owing to a rather large magnetic susceptibility difference with water and tissue. Collis et al[7] presented the technique of intramedullary nailing of a pathological humerus fracture with a radiolucent

carbon fibre nail. The radiolucent nail was made out of carbon fibre-reinforced polyether ether ketone. The nail had unique biomechanical properties that mimic the elasticity of the cortical bone and should result in the nail having a longer lifespan than a metal nail.

Despite these studies, some authors have suggested[9] that as the carbon fibre is an electrical conductor, there is a theoretical risk that local conductive current loops or antenna effects could cause it to heat up during MRI examinations.[10] In this work, we describe experiments that were designed to assess radio-frequency (RF) heating and MR image quality effects of a prototype three-section carbon fibre flatbed insert.

METHODS AND MATERIALS

Flatbed and MRI scanning

A carbon fibre flatbed insert for Philips MRI scanners (Philips Medical Systems, Best, Netherlands) was designed by the authors to have three separate panels for ease of manoeuvrability, setup and storage and manufactured by a specialist company (Norco GRP Ltd, Poole, UK). The central panel measures 0.77 × 0.52 m and each of the side panel measures 0.75 × 0.52 m (Figure 1). The central panel of the insert was designed to accommodate the bottom part of a 32-element body coil (16 elements in the anterior plane and 16 elements in the posterior plane) between the curved scanner bed and the insert. One of the side panels was designed with a cut-out on the side, allowing the coil cable to be connected to the scanner. The entire insert weighs approximately 7 Kg.

All experiments were carried out on a 3.0-T Achieva Tx MRI scanner (Philips Medical Systems, Best, Netherlands) in conjunction with a 32-element body coil.

Infrared thermometry

Measurements were carried out using a ThermoCAM® SC1000 thermographic camera (FLIR Infrared Systems Ltd, North Billerica, MA), which recorded a short-wave spectral band of 3.4–5.0 μm with a sensitivity of ±0.07 °C at 30 °C. Images of the MRI system and the insert were taken before and after dynamic imaging (32-element body coil) of mineral oil phantoms. A single axial slice was acquired dynamically through the centre of the phantom using three sequences with the following parameters: 50-mm slice thickness, 340 × 340-mm^2 field of view and 1-mm^2 in-plane resolution. The sequences were a spin-echo (SE) sequence [echo time (TE)/repetition time (TR) = 30/1000 ms run for 10 min], a turbo spin-echo (TSE) sequence (TSE factor 16, TE/TR = 30/1000 ms, run for 30 min) and a gradient-echo (GE) sequence (TE/TR = 4.1/7.5 ms, flip angle 10°, run for 10 min). The TSE sequence was run for a period of 30 min, as it uses a train of 180° refocusing RF pulses and hence the specific absorption rate (SAR) is higher.

Bragg-grating thermometry

To investigate heat deposition at the surface of the table, a tissue-mimicking phantom, which resembled an average human abdominal section, was made in a 300 × 300 × 120-mm^3 rounded square container using 7% bovine gelatine (Type B, SigmaAldrich) + 1% NaCl dissolved in 9 l of distilled water. The solution was heated to 45 °C using a hotplate and a magnetic stirrer was used to ensure that the powder-form gelatine dissolved uniformly in the water before being poured into the phantom container. The phantom was left overnight in a fridge at 4 °C in order to maximize its rigidity. The gelatine phantom was removed from the container and placed directly in contact with the carbon fibre flatbed insert. A 10-mm axial slice (field of view 320 mm, in-plane resolution 1 mm^2) through the middle of the phantom was acquired using three typical clinical sequences: a TSE (TSE factor 64, TE = 322 ms, TR = 2352 ms), a spoiled GE (flip angle 30°, TE = 4.3 ms, TR = 8.1) and a balanced GE (flip angle 90°, TE = 4.9 ms, TR = 9.8 ms) sequence. Each sequence was run for 10 min continuously. All sequences were set up with the shortest TE and TR possible, and the TSE length was also increased compared with standard imaging to increase SAR.

A four-channel Bragg-grating thermometry system, (Multitemp™ 4001; Optomed AS, Trondheim, Norway) with an accuracy of ±0.3 °C, was used to measure the temperature at the surface of the insert. This system has four optical fibre probes, each containing 10 Bragg gratings that are uniformly spaced 4-mm apart (centre to centre) so that there is a distance of 36 mm between the first and last grating. All 40 temperature measurement points were sampled at 5 Hz. The probes were inserted in the phantom in the locations indicated in Figure 2: 2 probes (Probes 1 and 3) were located in the axial imaging slice with Probe 1 inserted in the centre of the anterior plane while 3 probes (Probes 2–4) were placed as close as possible to the bed,

Figure 1. A prototype three-section carbon fibre flatbed insert: (a) top view and (b) underside view.

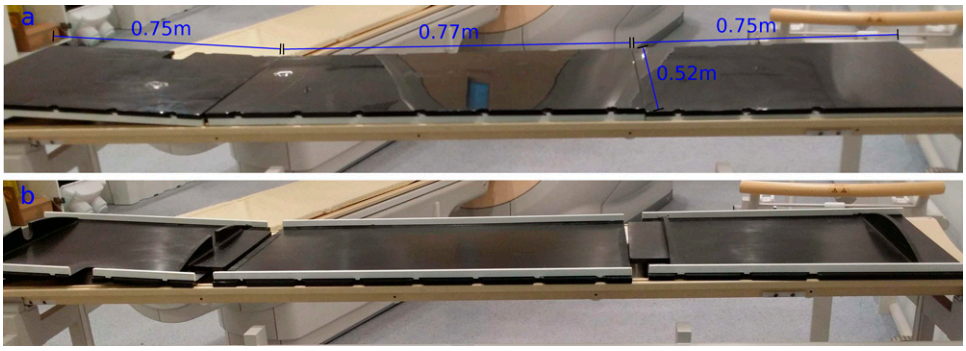

Figure 2. Experimental setup for the temperature measurement of the carbon fibre flatbed insert using the Bragg-grating thermometry system. The locations of the optical fibre probes are also shown. Two probes (Probes 1 and 3) are located in the axial imaging slice with Probe 1 inserted in the centre of the anterior plane, while three probes (Probes 2–4) are placed as close as possible to the bed with Probe 2 inserted in the left plane and probes (Probes 3 and 4) inserted in the right plane.

with Probe 2 inserted in the left plane and probes (Probes 3 and 4) inserted in the right plane. The phantom was left at room temperature with the probes recording baseline temperature for 15 min. Each sequence was run 3 times with a 1-min interval between each run.

Image quality

To assess image quality effects, images of mineral oil phantoms were acquired using the SE, TSE and GE sequences described in section Infrared Thermometry in Methods and Materials. Images were acquired with and without the flatbed insert in place and also with the scanner's MultiTransmit switch turned OFF and then ON. This switch uses multiple RF transmit/receive chains and coil elements in parallel, to improve RF uniformity in high-field MRI.[11] Two sets of phantom images were acquired, one set using the 32-element body coil and the other using the scanner's quadrature body coil. Phantom images were analyzed offline using the OsiriX software package (Pixmeo, Geneva, Switzerland). Regions of interest (ROIs) were placed over the largest mineral oil phantom and in the background of the image (10-cm-diameter ROI). Mean plus standard deviation values of pixel intensity were calculated for each of the three sequences. The signal-to-noise ratio (SNR) and percentage uniformity (U) were computed as follows:[3]

$$\mathrm{SNR} = {}^{S_{\mathrm{ROI}}}/_{\sigma_{\mathrm{Background}}}$$

$$U = \left(1 - \frac{\sigma_{\mathrm{ROI}}}{S_{\mathrm{ROI}}}\right) \times 100$$

where S_{ROI} is the mean signal intensity in the ROI and $\sigma_{\mathrm{Background}}$ and σ_{ROI} are the standard deviations of signal intensity in the background and ROI, respectively.

Images of the upper abdomen of a 40-year-old healthy male subject were acquired using a clinical TSE sequence (TE/TR = 80 ms/1171 ms, 2 signal averages, 5-mm slice thickness, TSE factor = 86), using the 32-element body coil and the scanner's quadrature body coil. Similar to phantom acquisition, images were acquired with and without the flatbed insert in place and also with the scanner's MultiTransmit switch turned OFF and then ON.

RESULTS

Infrared thermometry

Heat maps of the flatbed insert and the scanner bore are shown in Figure 3. All three sequences exhibited the same heating pattern, with the temperature of the scanner bore and the scanner table indicating an approximate offset of 1.5 °C above the room temperature. No heating was observed in the flatbed insert itself.

Bragg-grating thermometry

Temperature–time profiles for one run of the three sequences are shown in Figure 4. There was no sudden change in temperature on any of the probes and only small gradual increase in temperature (<0.2 °C) during a typical acquisition. The TSE sequence caused the largest temperature increase. This increase was measured by the probes located in the imaging plane.

Image quality

Acquired images of the mineral oil phantoms (experiment described in section Flatbed and MRI scanning in Methods and Materials) using the scanner's quadrature body coil configuration, without and with the flatbed insert in place and with the MultiTransmit switch set to OFF and then ON, are shown in Figure 5. SNR and signal uniformity were computed using the equations defined in section Image Quality in Methods and Materials and are presented in Table 1 for the 32-element body coil and in Table 2 for the scanner's body coil. For SE, TSE and GE sequences, the reduction in SNR was as much as 89% when the insert was in place compared with the standard couch, making it less suitable as a patient-support material. Turning on the MultiTransmit switch together with using the scanner's quadrature body coil improved the reduction in SNR from 89 to 39% for the SE sequence and from 82 to 12% for the TSE sequence. For the standard couch, improvement in SNR was as much as 29% for the SE sequence when the MultiTransmit switch was set to the "ON" state using the scanner's quadrature body coil. Turning on the MultiTransmit switch also improved signal uniformity with the carbon fibre insert in place compared with the standard couch. The drop in SNR and uniformity is more prevalent in the posterior part of the image (*i.e.* near the bed), specially when using the 32-element surface coil.

Example images of the upper abdomen of a healthy 40-year-old male volunteer are shown in Figure 6. The effect of shielding is evident, particularly in the posterior direction, where the posterior section of the 32-element body coil is located beneath the

Figure 3. Heat maps of the carbon fibre flatbed insert in (a), (b) and (c) following completion of the turbo spin-echo sequence. The bore of the scanner is captured in (c).

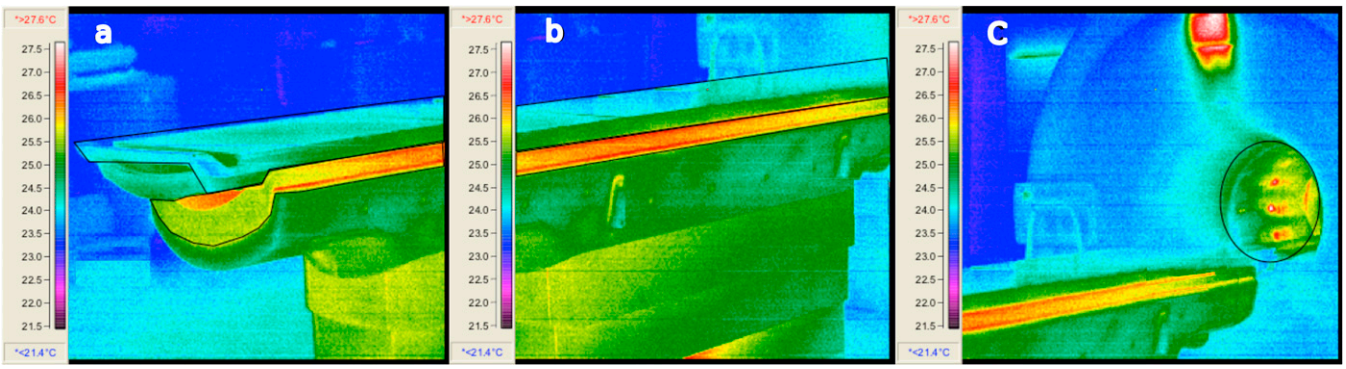

carbon fibre insert. Turning the MultiTransmit switch to the "ON" state also improved the image quality but not significantly for this particular coil configuration. Using the scanner's quadrature body coil resulted in noisier images compared with the 32-element body coil but with less shielding in the posterior section of the image.

DISCUSSION

In this work, we employed two different methods, namely an infrared thermometry system and a Bragg-grating thermometry system, to measure the temperature of a prototype carbon fibre flatbed insert during MRI examinations. The sampling frequencies of both techniques were positioned in the optical band of 60–86 THz and in the extremely low-frequency band of 3–30 Hz, respectively, thus avoiding interference with the scanner's RF fields.

In both experiments, we did not observe any heating or any sudden change of temperature, which could have indicated deposition of energy through current loops or antenna effects. The only changes observed were linked to RF energy deposition during imaging. The Bragg-grating thermometry system measured the largest temperature increase, when the TSE sequence was run. This result is unsurprising because SAR or the deposited RF energy in the subject is proportional to the square of the RF pulse flip angle being used[12] and the number of RF excitation pulses in a given time. The second highest temperature increase was measured when the balanced fast field echo (BFFE) sequence was run. No change in temperature was detected when the fast field echo (FFE) sequence was run. In conclusion, we found no evidence to support reports in the literature[9] regarding the heating of carbon fibre during typical MRI examinations.

The carbon fibre flatbed was found to be less suitable for MRI applications owing to it causing severe RF shielding artefacts, as reported in the Results section. This observation is consistent with a previous report, where the authors had to modify the design of a carbon fibre neonatal incubator owing to severe RF shielding artefact.[13] Two sets of phantom images were acquired, one set using the 32-element body coil and the other with the scanner's quadrature body coil. For SE, TSE and GE sequences, the reduction in SNR was as much as 89% when the insert was in place compared with the standard couch, making it less suitable as a patient-support material. Turning on the MultiTransmit switch together with using the scanner's quadrature body coil improved the reduction in SNR from 89 to 39% for the SE sequence and from 82 to 12% for the TSE sequence.

The use of the flatbed in radiotherapy warrants further investigation where conditions on image quality are less stringent compared with diagnostic imaging and images with reduced uniformity/SNR could potentially be sufficient for treatment

Figure 4. Temperature–time profiles during the acquisition of turbo spin-echo (TSE), balanced fast field echo (BFFE) and fast field echo (FFE) sequences.

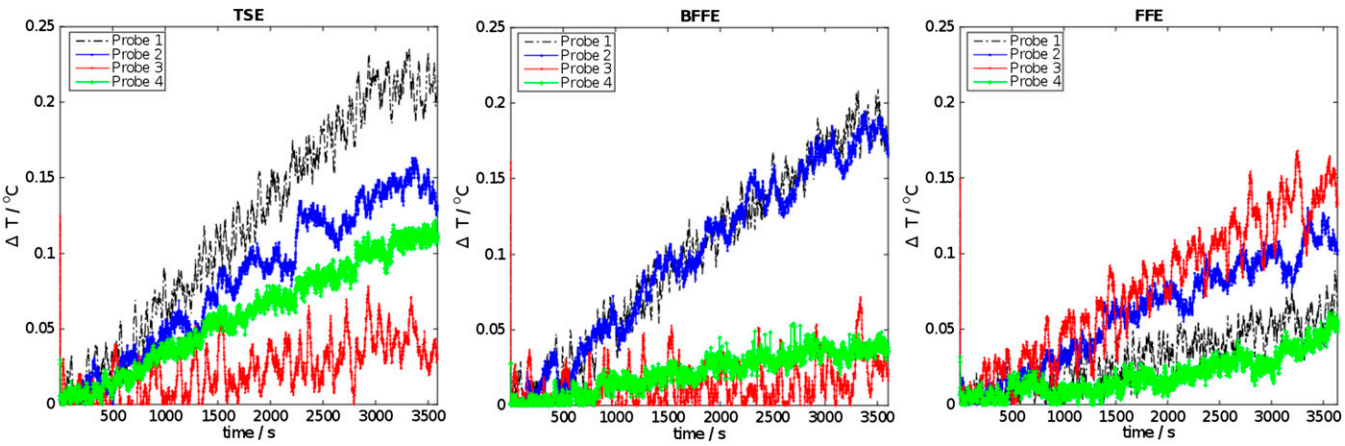

Figure 5. Axial images of mineral oil phantoms acquired without (row a) and with (row b) the carbon fibre flatbed insert in place for spin-echo (SE), turbo spin-echo (TSE) and gradient-echo (GE) sequences using the scanner's quadrature body coil and with the MultiTransmit switch (MX) turned OFF and then ON.

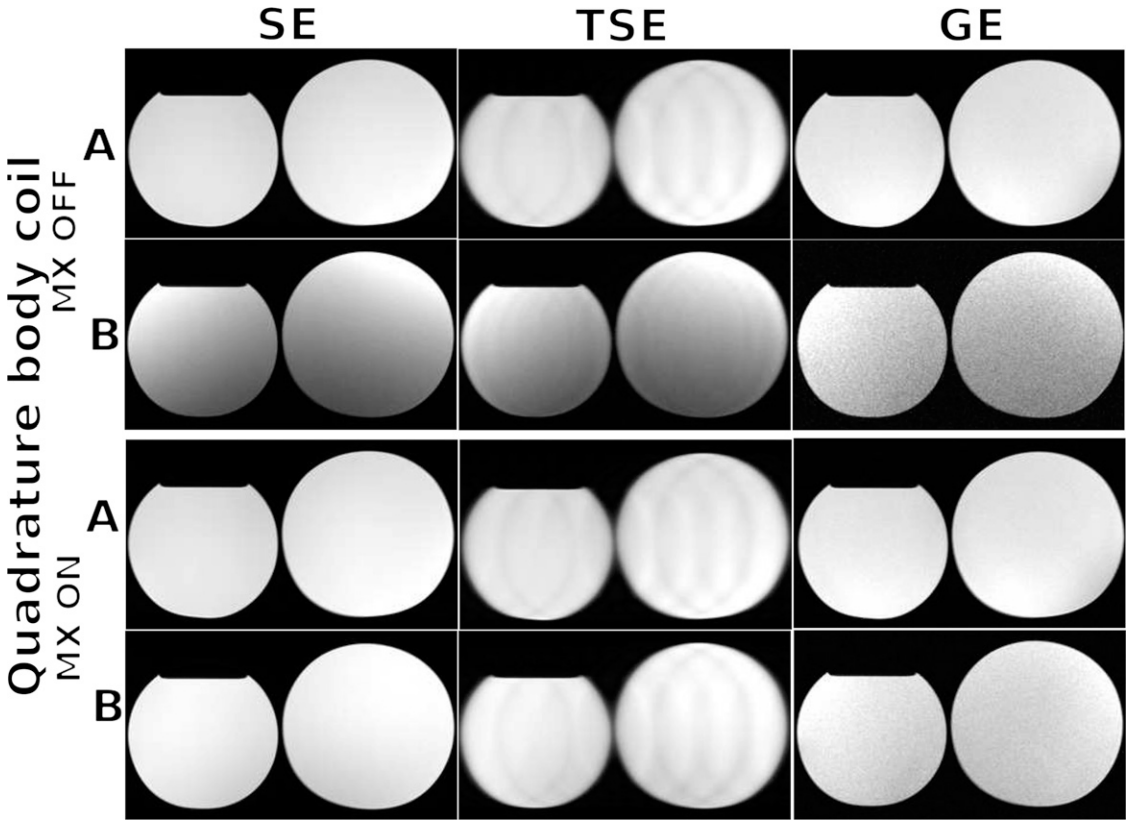

planning. The recommendations given by the American Association of Physicists in Medicine[14] and Institute of Physics and Engineering in Medicine[15] provide guidelines for image quality assurance in diagnostic radiology. In a recent work by Xing et al,[16] the authors demonstrated 40% reduction in SNR using a commercially available fibreglass flatbed specifically designed for treatment planning.

Potential applications of the carbon fibre flatbed in hybrid positron emission tomography (PET)/MRI[17] to support and immobilize patients must also be investigated. Despite significant advantages of hybrid PET/MRI,[18] the reproducibility of patient positioning remains a technical challenge, which must be overcome.[17] Devices inserted into the PET/MRI field of view cause attenuation of the PET signal,[17,19] a problem

Table 1. Percentage change in signal-to-noise ratio (SNR) and percentage uniformity (*U*) values without and with the carbon fibre insert in place for the spin-echo (SE), turbo spin-echo (TSE) and gradient-echo (GE) sequences with the MultiTransmit switch (MX) turned "OFF" and then "ON". The 32-element body coil configuration was used in this setup

RF transmission	Normal couch					
	SNR change (%)			*U* (%)		
	SE	TSE	GE	SE	TSE	GE
MX OFF	–	–	–	81	81	80
MX ON	+3	−3	+2	82	83	80
	Carbon fibre insert					
	SNR change (%)			*U* (%)		
MX OFF	−89	−82	−88	39	40	60
MX ON	−77	−65	−83	54	55	61

Table 2. Percentage change in signal-to-noise ratio (SNR) and percentage uniformity (*U*) values without and with the carbon fibre insert in place for the spin-echo (SE), turbo spin-echo (TSE) and gradient-echo (GE) sequences with the MultiTransmit switch (MX) turned "OFF" and then "ON". The scanner's quadrature body coil configuration was used in this setup

RF transmission	Normal couch					
	SNR change (%)			*U* (%)		
	SE	TSE	GE	SE	TSE	GE
MX OFF	–	–	–	96	96	96
MX ON	+29	−1.7	+0.87	97	96	96
	Carbon fibre insert					
	SNR change (%)			*U* (%)		
MX OFF	−80	−63	−82	74	74	86
MX ON	−39	−12	−64	95	95	94

Figure 6. Axial images of the upper abdomen of a healthy 40-year-old male subject without (row a) and with (row b) the carbon fibre flatbed insert in place using a clinical turbo spin-echo sequence. The 32-element body coil was used in this acquisition with the MultiTransmit switch (MX) turned OFF and then ON.

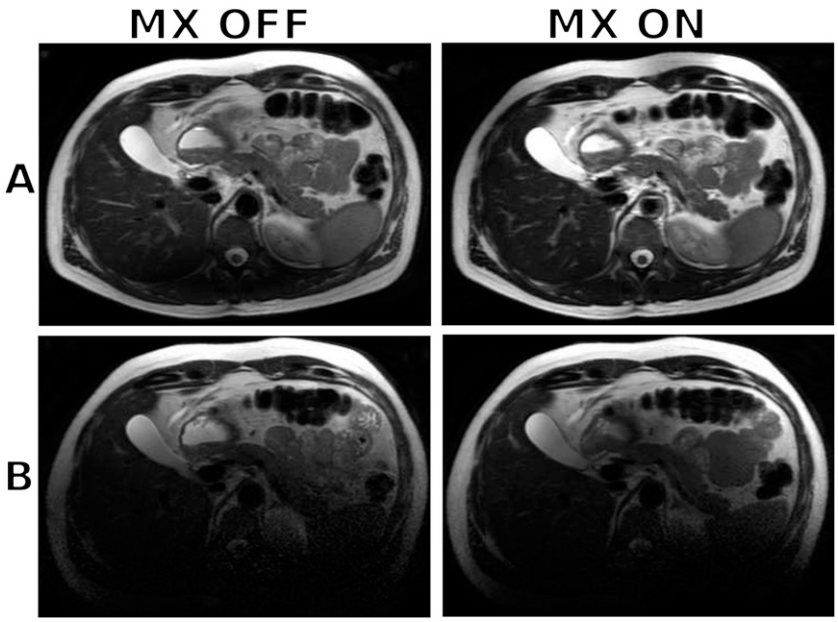

that must be addressed. Development of tools for patient positioning in hybrid PET/MRI systems presents a series of challenges, which require further research.

The Philips scanner used in this study employs two independent RF sources at 3.0 T.[20] It is well established that parallel RF transmission results in enhanced image uniformity, enhanced contrast uniformity, enhanced consistency (optimum RF shimming for each patient) and faster imaging.[11] This particular MultiTransmit switch is specific to the Philips Achieva 3.0-T scanner. At present, other vendors offer alternative RF shimming solutions. Siemens (Siemens Healthcare, Erlangen, Germany) offers a different anatomy-specific RF shimming solution referred to as "TimTX TrueForm" as part of the TimTX TrueShape architecture. GE (GE Healthcare, Waukesha, WI) offers MultiDrive RF Transmit with fully automated and independent RF pulse amplitude and phase control, to produce consistently clear 3.0-T images. Toshiba (Toshiba Medical Systems, Tokyo, Japan) offers multiphase transmission technology, which utilizes four points of RF transmission, combined with automatic adjustments in phase and amplitude, to ensure optimal RF distribution and homogeneity in all body regions.

One should also pay particular attention to the coil configuration used, when assessing RF shielding effects. This study demonstrated that using the scanner's quadrature body coil resulted in less reduction in SNR compared with the 32-element body coil, which could be attributed to the fact that the posterior section of the 32-element body coil was beneath the flatbed insert.

CONCLUSION

This study suggests that carbon fibre is less suitable for large-scale MRI applications owing to it causing severe RF shading. Further research is needed to establish the suitability of the flatbed for treatment planning using alternative sequences or whether an alternative carbon fibre composite for large-scale MRI applications can be found or if the shielding effect could be reduced by altering the design of the bed.

FUNDING

The authors gratefully acknowledge Barts Charity Grant 526/1463.

REFERENCES

1. DeMooy LG. The use of carbon-fibers in radiotherapy. *Radiother Oncol* 1991; **22**: 140–2. doi: http://dx.doi.org/10.1016/0167-8140(91)90010-E
2. Jockisch KA, Brown SA, Bauer TW, Merritt K. Biological response to chopped-carbon-fiber-reinforced peek. *J Biomed Mater Res* 1992; **26**: 133–46. doi: http://dx.doi.org/10.1002/jbm.820260202
3. Liney GP, Tozer DJ, van Hulten HB, Beerens EG, Gibbs P, Turnbull LW. Bilateral open breast coil and compatible intervention device. *J Magn Reson Imaging* 2000; **12**: 984–90. doi: http://dx.doi.org/10.1002/1522-2586(200012)12:6<984::AID-JMRI25>3.0.CO;2-X
4. Ernstberger T, Heidrich G, Bruening T, Krefft S, Buchhorn G, Klinger HM. The interobserver-validated relevance of intervertebral spacer materials in MRI artifacting. *Eur Spine J* 2007; **16**: 179–85. doi: http://dx.doi.org/10.1007/s00586-006-0064-5
5. Ernstberger T, Buchhorn G, Herbertbaums M, Heidrich G. In-vitro MRI detectability of interbody test spacers made of carbon fibre-reinforced polymers, titanium and titanium-coated carbon

fibre-reinforced polymers. *Acta Orthop Belg* 2007; **73**: 244–9.
6. Thomas C, Wojtczyk H, Rempp H, Clasen S, Horger M, von Lassberg C, et al. Carbon fibre and nitinol needles for MRI-guided interventions: first *in vitro* and *in vivo* application. *Eur J Radiol* 2011; **79**: 353–8. doi: http://dx.doi.org/10.1016/j.ejrad.2010.07.007
7. Collis PN, Clegg TE, Seligson D. The invisible nail: a technique report of treatment of a pathological humerus fracture with a radiolucent intramedullary nail. *Injury* 2011; **42**: 424–6. doi: http://dx.doi.org/10.1016/j.injury.2010.10.012
8. Hillock R, Howard S. Utility of carbon fiber implants in orthopedic surgery: literature review. *Reconstr Rev* 2014; **4**: 23–32.
9. Langmack KA. The use of an advanced composite material as an alternative to carbon fibre in radiotherapy. *Radiography* 2012; **18**: 74–7. doi: http://dx.doi.org/10.1016/j.radi.2012.02.001
10. Dempsey MF, Condon B, Hadley DM. Investigation of the factors responsible for burns during MRI. *J Magn Reson Imaging* 2001; **13**: 627–31. doi: http://dx.doi.org/10.1002/jmri.1088
11. Harvey PR, Hoogeveen RM. *MultiTransmit parallel RF transmission technology: setting the benchmark in clinical high-field imaging. Tech. rep*. Netherlands: Philips Healthcare; 2009.
12. McRobbie DW, Moore EA, Graves MJ, Prince MR. *MRI from picture to proton*. 2nd edn. Cambridge, UK: Cambridge University Press; 2006.
13. Paley MN, Hart AR, Lait M, Griffiths PD. An MR-compatible neonatal incubator. *Br J Radiol* 2012; **85**: 952–8. doi: http://dx.doi.org/10.1259/bjr/30017508
14. Och JG, Clarke GD, Sobol WT, Rosen CW, Mun SK. Acceptance testing of magnetic resonance imaging systems: report of AAPM nuclear magnetic resonance task group no. 6. *Med Phys* 1992; **19**: 217–29. doi: http://dx.doi.org/10.1118/1.596903
15. Fransson A. IPEM Publication, Report No. 80-Quality control in Magnetic Resonance Imaging, R. Lerski, J. de Wilde, D. Boyce, J. Ridgway, Institute of Physics and Engineering in Medicine, UK, 1999. ISBN 0-904181 901. *Eur J Radiol* 2000; **36**: 59–60. doi: http://dx.doi.org/10.1016/S0720-048X(99)00162-X
16. Xing A, Holloway L, Arumugam S, Walker A, Rai R, Juresic E, et al. Commissioning and quality control of a dedicated wide bore 3T MRI simulator for radiotherapy planning. *Int J Cancer Ther Oncol* 2016; **4**.
17. Thorwarth D, Leibfarth S, Monnich D. Potential role of PET/MRI in radiotherapy treatment planning. *Clin Transl Imaging* 2013; **1**: 45–51. doi: http://dx.doi.org/10.1007/s40336-013-0006-2
18. Zaidi H, Ojha N, Morich M, Griesmer J, Hu Z, Maniawski P, et al. Design and performance evaluation of a whole-body Ingenuity TF PET-MRI system. *Phys Med Biol* 2011; **56**: 3091–106. doi: http://dx.doi.org/10.1088/0031-9155/56/10/013
19. Mantlik F, Hofmann M, Werner MK, Sauter A, Kupferschlager J, Scholkopf B, et al. The effect of patient positioning aids on PET quantification in PET/MR imaging *Eur J Nucl Med Mol Imaging* 2011; **38**: 920–9. doi: http://dx.doi.org/10.1007/s00259-010-1721-9
20. Harvey PR, Prins WM, Zhai Z, Fuderer M, Van YGH, inventors. Adjustment of RF-field homogeneity in high-field MR imaging. Patent WO2006033047. 2006.